Simulation of Electron Kinetics in Gas Discharges

Vladimir I. Kolobov and Robert R. Arslanbekov

Abstract—**We review the state-of-the-art for the simulation of electron kinetics in gas discharges based on the numerical solution of the Boltzmann equation. The reduction of the 6D Boltzmann equation to a 4D Fokker-Planck equation using two-term spherical harmonics expansion enables efficient and accurate simulation of the electron distribution function in collisional gas discharge plasmas. We illustrate this approach in application to inductively coupled plasmas, capacitively coupled plasmas, and direct current glow discharges. The incorporation of the magnetic field effect into this model is outlined. We also describe recent efforts towards simulating collisionless effect in gas discharge plasma based on Vlasov solvers and outline our views on future development of the numerical models for gas discharge simulations.**

Index Terms—**Electron kinetics, Boltzmann, Fokker Planck, Vlasov equations, Inductively Coupled Plasma, Capacively Coupled Plasma, Positive Column, Striations**

I. INTRODUCTION

Gas discharge plasma represents an extremely non-equilibrium system where electron mean energy (temperature) exceeds gas temperature by two orders of magnitude. The electron distribution function (EDF) is formed as a result of electron heating by electromagnetic fields and collisions with neutral atoms, it deviates from an equilibrium (Maxwellian) distribution in most cases. Solution of the Boltzmann kinetic equation for electrons becomes crucial for accurate simulation of the plasma since many phenomena cannot be properly understood without kinetic analysis [1],[2]. Fortunately, substantial simplification of the electron Boltzmann equation is possible due to a large disparity of electron and atom masses. Due to this mass disparity, the electron energy relaxation in elastic collisions with atoms occurs much slower than momentum relaxation. As a result, the EDF is weakly anisotropic in velocity space and can be presented as a sum of a large isotropic part f_0 and a small addition f_1.

Furthermore, three different cases can be distinguished. In the case of large pL and small E/p (where p is the gas pressure, L is the characteristic scale of the plasma, and E is the electric field), the spatial gradients are small and both f_0 and f_1 are determined by local values of the electric field, electron density, and plasma composition. The electrons can be described by continuum (fluid) equations with transport coefficients derived from the local (non-Maxwellian) EDF. A typical example of such plasmas is dielectric barrier discharges (DBD) and other atmospheric pressure plasma sources described in a recent review [3]. The local Boltzmann solvers are being used more frequently to obtain electron transport coefficients and reaction rates for fluid models [4],[5].

The second case corresponds to a collisional plasma where L is much larger than electron mean free path λ but is comparable to electron energy relaxation length λ_ε. The latter can exceed λ by orders of magnitude due to small ratio of the electron to atom masses. In this non-local regime, the isotropic part of the EDF, f_0, at a given point depends not only on the electric fields at this point but also by plasma properties in the vicinity of the point of the size λ_ε (a memory effect). The anisotropic part f_1 is a local function of the field (local electrodynamics). In this collision-dominated regime, the plasma cannot be described by hydrodynamics, and a number of interesting phenomena caused by non-local electron kinetics take place [6]. The most typical example is ionization waves (striations) in the positive column of direct current (DC) glow discharges important for fluorescent lamps and gas lasers.

With further decrease of pL, the electron mean free path becomes comparable or larger than the characteristic size of the plasma. In this nearly collisionless regime, the anisotropic part f_1 at a point is determined not only by the local value of the electric field at this point, but also by the profile of the electric field in the vicinity of the point of size λ along the electron trajectory. As a result, the local relationship between the current density and the electric field (Ohm's law) becomes invalid. This is the area where gas discharge physics meets fusion plasma physics which is traditionally focused on collisionless phenomena and hot plasma effects [7]. Plasma reactors used for modern semiconductor manufacturing frequently operate in this regime [8].

The importance of electron kinetics in gas discharges has been recognized and emphasized in a number of review papers [9],[10]. Over the last decade, considerable progress has been achieved in simulations of electron kinetics and self-consistent modeling of gas discharges [11],[12],[13]. In this paper, we review recent progress in the numerical solution of the electron Boltzmann equation and outline future directions for scientific research and development of software tools for computer aided engineering of plasma devices and processes. We focus our attention on deterministic methods of solving the Boltzmann equation, and only briefly mention statistical particle simulation methods reviewed in [14],[15].

II. BASIC EQUATIONS

A. Boltzmann Equation and its Derivatives

The Boltzmann transport equation (BTE) describes the evolution of a particle distribution function $f(\mathbf{r},\mathbf{v},t)$ in a six-dimensional phase space [16]

$$\frac{\partial f}{\partial t} + \nabla_r \cdot (\mathbf{v}f) + \nabla_v \cdot (\mathbf{a}f) = I \qquad (1)$$

Here $\mathbf{r}$ is a position vector in physical space, $\mathbf{v}$ is the velocity vector, $\mathbf{a}$ is the acceleration vector and t is time. The right hand side of Eq. (1) contains an integral operator in velocity space describing binary collisions among particles. Integrating $f(\mathbf{r},\mathbf{v},t)$ over velocity space gives particle density, $n(\mathbf{r},t)$.

For weakly ionized plasmas, electron collisions with neutrals usually dominate over collisions among charged particles.. Due to disparity of electron/atom mass ($m/M \ll 1$), the Boltzmann collision integral for elastic collisions of electrons with heavy neutrals can be written in the so-called Lorentz-gas form [17],[18]

$$\begin{aligned} I_{el} = &-\frac{1}{v^2}\frac{\partial}{\partial v}v^2\Gamma - \\ &Nv\int_{S^2}\sigma(v,|\Omega-\Omega'|)\big[f(v,\Omega')-f(v,\Omega)\big]d\Omega \end{aligned} \qquad (2)$$

where Ω is the velocity angle on a unit sphere S^2 in velocity space ($\mathbf{v}=v\Omega$), and σ is the collision cross section, and N is the gas density. The flux Γ is given by

$$\Gamma = -\frac{\delta v}{2}\left(vf + \frac{T}{m}\frac{\partial f}{\partial v}\right)$$

where T is the gas temperature, v is the transport collision frequency and $\delta = \dfrac{2m}{M}$ is the average fraction of the energy lost by the electrons in one elastic collision. The first term in (2) is small and describes energy exchange between electrons and neutrals. The second, leading term in (2) describes collisions with infinitely heavy particles which tend to isotropize the electron distribution but do not change their energy. Thus, due to mass disparity, electron momentum relaxation in elastic collisions occurs much faster than energy relaxation, and the EDF averaged over velocity angles evolves on a time scale $\tau_u \sim \tau M/m$, much slower than evolving the complete distribution. Inelastic processes do not change this picture if characteristic energy of electrons is small compared to inelastic threshold [19].

For collisional plasmas, a two-term spherical harmonics expansion (SHE) of the EDF in velocity space is commonly used [20],[21]

$$\mathbf{f}(\mathbf{r},\mathbf{v}.t) = f_0(\mathbf{r},v,t) + \frac{\mathbf{v}}{v}\cdot\mathbf{f}_1(\mathbf{r},v,t) \qquad (3)$$

This approximation results in two coupled equations for f_0 and $\mathbf{f}_1$ (sometimes called Davydov-Allis system):

$$\frac{\partial f_0}{\partial t} + \frac{v}{3}\text{div}(\mathbf{f}_1) + \frac{1}{3v^2}\frac{\partial}{\partial v}\left(v^2\frac{e\mathbf{E}}{m}\cdot\mathbf{f}_1\right) = S_0 \qquad (4)$$

$$\frac{\partial \mathbf{f}_1}{\partial t} + v\mathbf{f}_1 = -v\nabla f_0 - \frac{e\mathbf{E}}{m}\frac{\partial f_0}{\partial v} \qquad (5)$$

Here, e and m are the unsigned charge of an electron and electron mass, $\mathbf{E}$ is electric field vector, S_0 is the collision integral involving energy exchange in elastic and inelastic electron-atom collisions and electron-electron interactions. It is seen from (5) that the two-term approximation results in Ohm's law because $\mathbf{f}_1$ depends on local value of the electric field. The accuracy of the two-term SHE for electron swarms and plasmas is discussed in [22]. Even in situations where its applicability is not obvious, the two-term SHE gives unexpectedly good results [23].

For many cases, Eq. (5) can be resolved for $\mathbf{f}_1$ and substituted into (4). Dividing the electric field into a potential and vortex components, $\mathbf{E}=-\nabla\phi-\partial\mathbf{A}/\partial t$, where ϕ is the electric potential and $\mathbf{A}$ is the vector magnetic potential, and using the Volt-equivalent of the kinetic energy $u=mv^2/2e$ as the independent variable, one obtains a single closed equation for the Electron Energy Probability Function (EEPF) f_0 in the form

$$\begin{aligned} &\frac{\partial f_0}{\partial t} - \nabla\cdot\left[D_r\left(\nabla f_0 + \nabla\phi\frac{\partial f_0}{\partial u}\right)\right] - \\ &\frac{1}{\sqrt{u}}\frac{\partial}{\partial u}\left[\sqrt{u}D_r\nabla\phi\cdot\left(\nabla f_0 + \nabla\phi\frac{\partial f_0}{\partial u}\right) + \sqrt{u}\left(V_u f_0 + D_u\frac{\partial f_0}{\partial u}\right)\right] \\ &= S \end{aligned} \qquad (6)$$

Different terms in Eq. (6) describe, correspondingly, the diffusion in physical space (second term), with a diffusion coefficient $D_r = v^2/3v$, the electron drift and heating

(cooling) due to the electrostatic field (third term); quasi-elastic processes (third term) represented by the convection and diffusion along the energy axis with a convection velocity V_u and a diffusion coefficient in energy D_u. The quasielastic processes include elastic collisions of electrons with neutrals, excitation of molecular vibrations, Coulomb interactions among electrons and ions, and electron heating by electromagnetic fields. Strongly inelastic collisions (excitation, ionization, attachment, etc.) are described by the right hand side of Eq (6). Specific expressions for S and $\delta(u)$ can be found, for instance, in [24].

The Fokker Planck Equation (FPE) (6) appears as an intermediate step between the BTE (1) and continuum models for the time scales exceeding collision time τ and for spatial scales exceeding the mean free path λ. Numerical methods of solving FPE in the form (6) were developed in [25],[26].

It is often convenient to use *total* energy $\varepsilon = u - e\phi(\mathbf{r},t)$ as the independent variable instead of *kinetic* energy u. In this case, the FPE (6) can be written in the form [27],[28]:

$$\frac{\partial f_0}{\partial t} - \frac{\partial \phi}{\partial t}\frac{\partial f_0}{\partial \varepsilon} - \nabla \cdot D_r \nabla f_0 -$$
$$\frac{1}{\chi}\frac{\partial}{\partial \varepsilon}\left(\chi\left[D_\varepsilon(\mathbf{r},\varepsilon)\frac{\partial f_0}{\partial \varepsilon} + V_\varepsilon(\mathbf{r},\varepsilon)f_0\right]\right) = S \quad (7)$$

where $D_\varepsilon(\mathbf{r},\varepsilon) = D_u(\mathbf{r}, u - e\phi)$, $V_\varepsilon(\mathbf{r},\varepsilon) = V_u(\mathbf{r}, u - e\phi)$. It is seen that using *total* energy eliminates complicated cross-derivative terms in Eq. (6). The price for this simplification is more complex boundary conditions for Eq. (7) which have to be specified at curved boundaries in the $(\mathbf{r},\varepsilon)$ space (see Figure 1). One of the boundaries corresponds to zero kinetic energy and is defined by the equation $\varepsilon = -e\phi(x,t)$. At this boundary, zero flux of particles is usually assumed. The boundary condition at ε_{max} corresponds to $f_0 = 0$. The commonly used boundary condition in physical space at absorbing boundaries is of the form

$$v f_0 \frac{\delta\Omega}{4\pi} = -D_r \frac{\partial f_0}{\partial x} \quad (8)$$

where $\delta\Omega = 2\pi\left(1 - \sqrt{e\varphi_w/\varepsilon}\right)$ is the loss cone, and φ_w is the potential value at a distance λ from the boundary. The boundary condition at electron-emitting boundaries is

$$-\lambda \frac{\partial f_0}{\partial x} = \Phi(\varepsilon)$$

where function $\Phi(\varepsilon)$ is determined by the near-electrode processes (see, for instance, [29]).
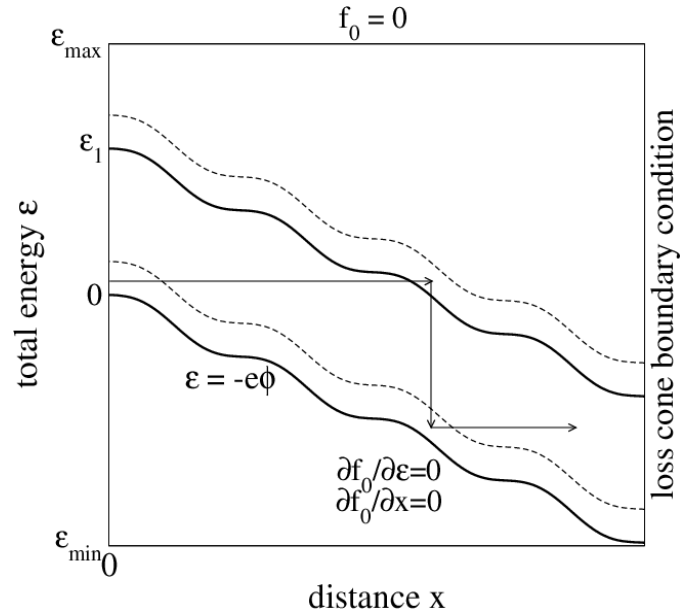

Figure 1. An example of computational domain and boundary conditions for Eq. (7). Arrows show a typical trajectory of an electron emitted from the boundary at $x=0$. Inelastic collisions correspond to a jump along the energy axis at a given point in space.

In our simulations, we used a uniform mesh along the ε axis and arbitrary mesh in physical space. It is possible to mesh only the band $-e\phi(x) < \varepsilon < -e\phi(x) + \varepsilon_{max}$ and use a non-uniform grid in ε as in [30]. This could save computer memory for problems where potential variation is large compared to the typical kinetic energy of electrons, such as the positive column of a DC discharge in a long tube.

B. Self-consistent discharge simulation.

For self-consistent plasma simulations, the transport and chemistry of charged and neutral particles have to be calculated in a coupled manner with electromagnetic fields. Often, it is possible to enforce quasi-neutrality by assuming zero electron current in the plasma. From Eq. (6), this condition gives the electric field in the current-free plasma [25]

$$\mathbf{E} = -\frac{\int d\mathbf{v}\, v^2 D_r \nabla f_0}{\int d\mathbf{v}\, v^2 D_r \frac{\partial f_0}{\partial u}} \quad (9)$$

An alternative approach for calculation of the electric field is to use charge conservation [31] or solve the Poisson equation [32]. Details of our implementation of a hybrid plasma solver can be found in [33]. Below, we give only a brief outline of the important features.

The electrostatic potential for transient simulations has been obtained from the following equation (see [34] and references therein)

$$\nabla \cdot (\varsigma + \mu_e n_e \Delta t) \nabla \phi(t + \Delta t) = e \left[n_e - \sum_i q_i n_i \right] - e \Delta t \nabla \cdot D_e \nabla n_e \tag{10}$$

where ς is the electrical permittivity of the medium, μ_e and D_e are the electron mobility and diffusion coefficients, n_e and n_i are the electron and ion densities, q_i is the sign of *i*-ion charge and Δt is the time step of transient simulations. Equation (10) is solved in the entire domain, including plasmas, dielectrics, and conductors. The surface charges on dielectric surfaces are calculated from fluxes of ions and electrons to the surface. For $\Delta t \rightarrow 0$, Eq. (10) is reduced to the Poisson equation, for $\Delta t \rightarrow \infty$, it expresses the conservation of electron current, $\nabla \cdot \mathbf{j}_e = 0$. Employing Eq. (10) for calculation of the electrostatic potential allows using time steps much larger than the time steps dictated by CFL criteria, $\Delta t < (e\mu_e n_e)^{-1}$.

For calculation of electron density in (10), the electron balance equation is solved together with the kinetic equation (7), using the electron production rate and electron flux provided by the kinetic module. The electron number density calculated this way is also used in Maxwell equations for calculations of the vector magnetic potential **A**.

The ion density has been found by solving continuum equations with either a drift-diffusion approximation for the ion flux or by solving a momentum equation for the ion drift velocity. Usually, the ion velocity distribution is strongly anisotropic and the ion drift velocity exceeds the thermal ion velocity. Ion temperature is assumed to be equal to gas temperature in our calculations.

Different FP approaches to simulate electron transport in plasmas are compared in [35]. Details of our numerical FPE solution can be found in [36] [37].

C. Including magnetic field and electron inertia

When a static magnetic field is included in the two-term SHE approximation, Eq. (5) becomes.

$$\frac{\partial \mathbf{f}_1}{\partial t} + \nu \mathbf{f}_1 - \boldsymbol{\omega}_B \times \mathbf{f}_1 = -\mathbf{v} \nabla f_0 - \frac{e\mathbf{E}}{m} \frac{\partial f_0}{\partial \mathbf{v}} \tag{11}$$

where $\boldsymbol{\omega}_B = e\mathbf{B}/m$ is the electron cyclotron frequency vector. An implicit 2D solver for Eqs. (4) and (11) with account of self-consistent magnetic field and electron inertia was developed in [38]. A similar approach was used in [39] for studies of spatial relaxation of electrons and in [40] for simulation of magnetron discharges. Electron kinetics in RF electric and magnetic fields was discussed in [41].

D. Solution of the Vlasov Equation

In the absence of collisions, Equation (1) is called the Vlasov equation. Vlasov solvers have been used for studies of collisionless plasmas as an alternative to PIC methods. Recently, these solvers have been also applied to simulation of gas discharge plasmas. A recent review of Eulerian Vlasov solvers can be found in [42].

III. SIMULATION OF COLLISIONAL PLASMAS

A. Inductively Coupled Plasmas

Among different plasma sources, Inductively Coupled Plasma (ICP) is probably the simplest for the numerical solution. Due to the small thickness of the space charge sheaths at plasma boundaries, a good solution can be obtained using quasineutral approximation (9) for calculation of the electrostatic potential in the plasma. As a next step, the sheath structure can be resolved using non-uniform mesh near the boundaries. For typical driving frequency of 13.56 MHz, there is no need to resolve the RF period since all the plasma parameters vary slightly during the RF period.

We will demonstrate typical results of 2D self-consistent simulations of ICP for the experimental system studied in detail by Godyak's group over the last several years (see [43],[44] and references therein). The experimental setup and electrical characteristics of this system are described in [43]. The plasma is created in a cylindrical chamber of radius *R*=10 cm and length *L*=10.5 cm driven by a planar 5-turn coil separated from the dielectric window by the Faraday shield. With good accuracy, the system is axially symmetric and 2D simulations are sufficient. Experimental data for this system is available [44] for a wide range of operating conditions (pressure 0.3-100 mTorr, power absorbed in plasma 12-200W, driving frequency 0.45-13.56 MHz). Figure 2 shows the calculated spatial distributions of electron temperature (left) and electrostatic potential (right) for 10 mTorr, 6.8 MHz, 100 W. It is worth noting the minimum of electron temperature in the center of the reactor, which cannot be explained by fluid models.
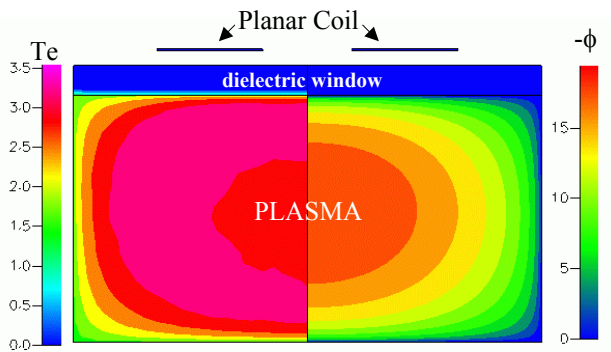

Figure 2. Calculated electron temperature (left) and electrostatic potential (right) for 10 mT, 6.8 MHz, 100W.

The model included 4 plasma species: Ar (ground state), Ar^* and Ar^{**} (two metastable states with energies $u^* = 11.55$ eV and $u^{**} = 13.2$ eV, correspondingly), radiation transitions from Ar^{**} to Ar^* states, direct, stepwise and Penning ionization, according to [45]. The ion inertia effect was shown to play an important role for gas pressure below 10 mTorr. The electrostatic potential was found by solving Eq. (10) using spatially non-uniform mesh to resolve the sheath structure near the boundaries. The surface charge on dielectrics was found from the local balance of electron and ion fluxes. The boundary condition for the EEDF at the walls was defined according to Eq. (8).

The measured and calculated EEPFs [46] are shown in Figure 3 as functions of total electron energy in different points along the discharge axis at radius r=4 cm where the induced electric field reaches maximal value. It is seen that the body of the EEPF depends solely on total electron energy, and the EEPF tail is enhanced by hot electrons near the coil due to electron heating, in accordance with the experiments. Similar results were obtained for a different system in a series of publications by Kortshagen et al. (see [47], [48], [49] and references therein) using a similar computational approach, and for the same system by Vasenkov & Kushner [45] using Monte Carlo simulations of electrons. It should be noted the EEPF deviates from the Maxwellian even for highest plasma densities obtained in this system. The electron induced reaction rates are very sensitive to the "tail" of the EEPF and assumption of a Maxwellian EEPF can result in large errors in calculation of electron induced reaction rates.
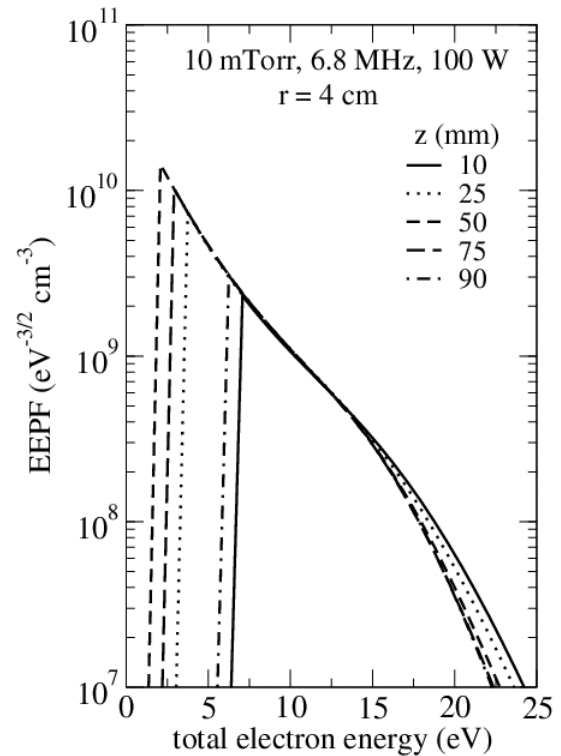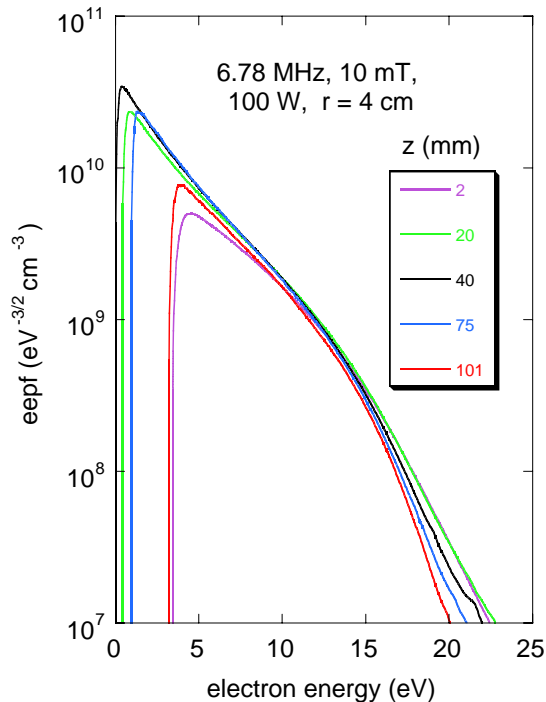

Figure 3. EEPFs at different points along the discharge axis at radial position r=4 cm (after Ref. [46]): a) measured, b) calculated.

The calculated axial distributions of electron temperature T_e and plasma potential are compared in Figure 4 with the experimental data [44]. The electron temperature is defined as $T_e = 2 \langle u \rangle / 3$, where $\langle u \rangle$ denotes the mean kinetic energy.
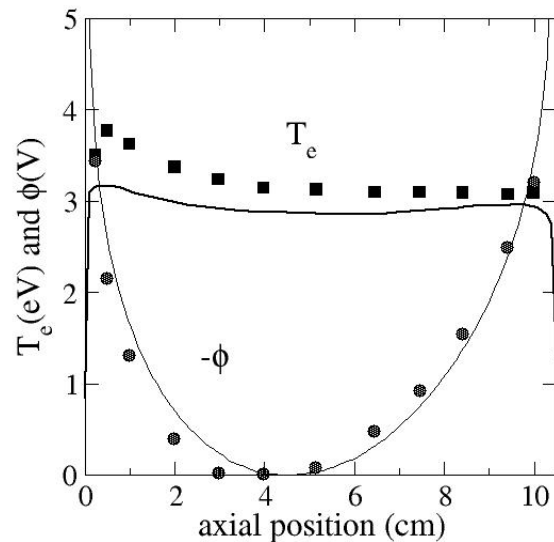

Figure 4. Experimental (points) and simulated (lines) electron temperature and plasma potential along the discharge axis at $r = 4$ cm.

Gas heating affects plasma parameters in ICP even for moderate input powers [50], [51]. Spatially non-uniform gas heating occurs due to ion and electron collisions with neutrals in the bulk plasma and heat release at surfaces due to ion bombardment and surface reactions. Figure 5 shows the calculated gas temperature in the center of the reactor as a function of the power absorbed in plasma for different gas pressures [46].
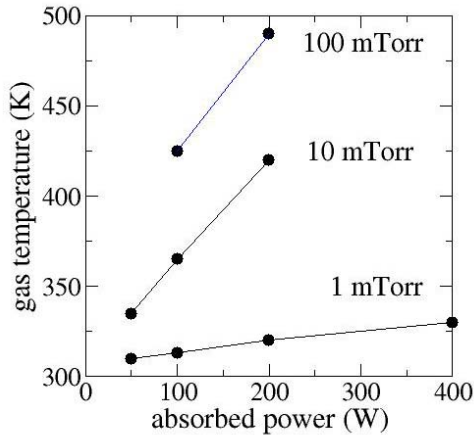

Figure 5. Calculated gas temperature in the center of plasma as a function of absorbed power for different gas pressures

With the decrease of driving frequency, oscillations of plasma parameters during RF period become noticeable. The origin of these oscillations can be easily understood by assuming that the induced electric field in ICP has a single time-harmonic component with angular frequency ω. Then, the part of the diffusion coefficient in energy $D_\varepsilon(\mathbf{r}, \varepsilon)$ in Eq. (7) caused by electron heating has the form [52]

$$D_E = D_{E0}\left(1 + \cos(2\omega t) + \frac{\omega}{\nu}\sin(2\omega t)\right) \quad (12)$$

where $D_{E0} = \frac{\nu^2}{6\nu}\frac{E_{rf}^2(\mathbf{r})}{\left(1 + (\omega/\nu)^2\right)}$, and $E_{rf}(\mathbf{r})$ is the amplitude of the inductive RF electric field. The time variation of the diffusion coefficient is the primary reason for oscillations of the electron temperature, trapping potential, and the excitation/ionization rates. Figure 6 shows an example of time modulation of electron temperature for the ICP reactor [43] in Argon, at gas pressure p=10 mTorr, RF frequency 450 kHz in three different points x=9, 5, and 1 cm along the discharge axis from the coil location. It is seen that oscillations occur at the second harmonic of the driving frequency, and there is a phase shift between the oscillations at different points. The modulation of EEPF occurs mainly in the tail and is more pronounced near the coil where electron heating takes place. The knowledge of the EEPF could be useful in the optical emission spectroscopy of discharges [53], [54].
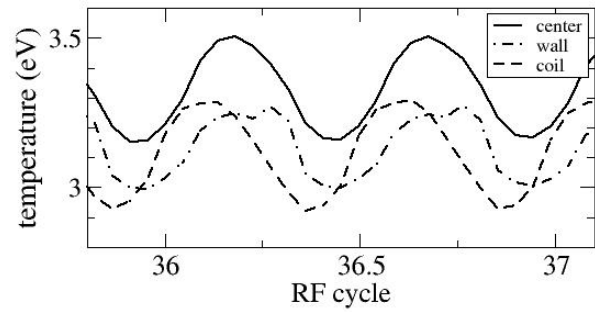

Figure 6. The time variation of the electron temperature at three locations along the discharge axis at r=4 cm.

Finally in this section, we present an example of pulsed power simulations for the same reactor in Argon gas, at 10 mTorr, 6.8 MHz, for a pulse-modulated coil current of 50-400 A. The pulse duration varied in the range 30 and 50 μs, the repetition rate is 100 μs. Figure 7 shows the time variation of the electron temperature, metastable Ar* density, and electron density in the center of the discharge chamber. Figure 8 shows the time variation of the EEPF and the wall potential (vertical lines). It is seen that a sharp increase of the electron temperature at the beginning of the active phase results in excessive production of metastable atoms during this phase. The electron production during this time is mainly due to Penning ionization:
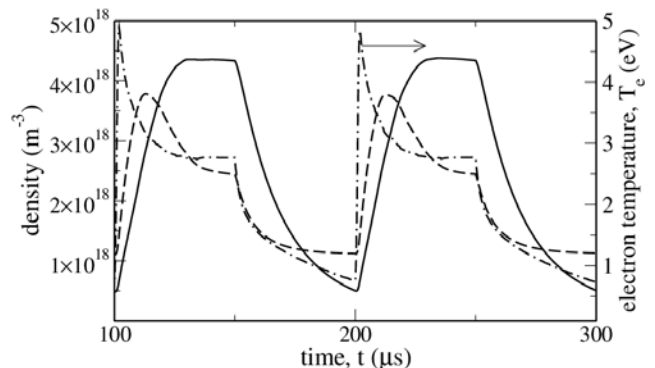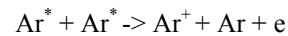
$$Ar^* + Ar^* \rightarrow Ar^+ + Ar + e$$

Figure 7. The time variation of electron temperature, electron density, and metastable density in pulsed ICP.
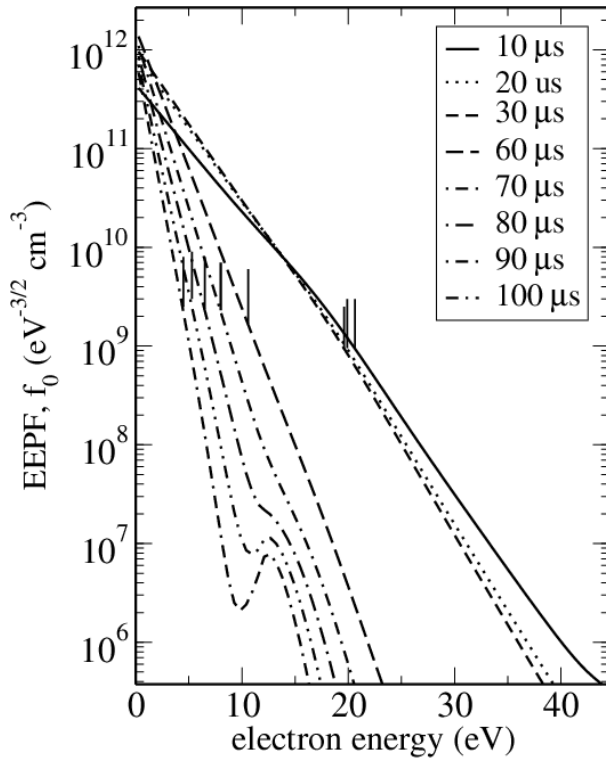
Figure 8. The time variation of the EEPF and the wall potential (vertical lines) in pulsed ICP. Times are shown relative to the beginning of the pulse.

In the afterglow, the EEPF body is Maxwellian and is depleted at energies higher than the wall potential (see Figure 8). A pronounced peak at ~12 eV is formed due to rapid electron production in collisions of slow electrons with metastable atoms. Such a behavior is typically observed in experiments for similar ICP systems [55], [56]. The presence of energetic electrons can dramatically effect the potential distribution and the wall potential in the low-pressure afterglow plasma [57].

B. Capacitively Coupled Plasmas

Anatomy of Capacitively Coupled Plasma (CCP) is described in detail in [58], [59]. The mechanism of electron heating in CCP in weakly collisional regimes remains a subject of active research [60]. Among other research topics are electron inertia effects at ultra-high frequencies [61],[62] and standing wave effects in large area CCP sources [63],[64] important for practical applications.

For simulations of CCP, we use total energy with **instantaneous** potential (TEIP) formulation. In this formulation, electron heating in RF sheaths occurs due to interactions with moving boundaries, defined by the equation $\varepsilon = -e\phi(\mathbf{r},t)$. Figures 9 and 10 illustrate the mechanism of electron heating by the electrostatic potential in the form

$$\phi(x,t) = \begin{cases} A(x-s)^2, & 0 < x < s(t) \\ 0 & L > x > s(t) \end{cases} \qquad (13)$$

where $s(t) = s_0(1 + \cos(\omega t))$. A Maxwellian EEPF is assumed at $x=L$, the boundary condition of the type (8) is assumed at $x=0$. The collision cross sections for Argon are used and the ionization is turned off. Figures 9 and 10 show results of simulation for $A = -4\times10^6$, $s_0 = 0.25$ cm, $L = 1$ cm, frequency 10 MHz, gas pressure $p = 200$ mTorr for two different cases. For the first case, the term with $\partial\phi/\partial t$ in Eq. (7) was turned off, for the second case this term was included in the simulation. The comparison of these Figures shows that the transient term in Eq. (7) plays an important role in the heating process and the formation of the EEPF. This term describes the "drift" of electrons along total energy by virtue of time varying potential. In other words, due to time variation of potential energy, electrons are being "pushed" up or down along the total-energy axis depending on the sign of $\partial\phi(\mathbf{r},t)/\partial t$ at a given point. This term simply compensates the shift of the energy reference point. Indeed, if we shift ε by some value $d\varepsilon$, the particle's positions and velocities remain unchanged. Also the EEPF has to be the same, in the phase space $(\mathbf{r},\varepsilon)$, shifted in new variables by $d\varepsilon$. The term with $\partial\phi(\mathbf{r},t)/\partial t$ in the kinetic equation simply compensates for this shift of the phase space. In general, the neglect of this term gives an error since the kinetic equation in the total energy domain is algebraically wrong without this term.
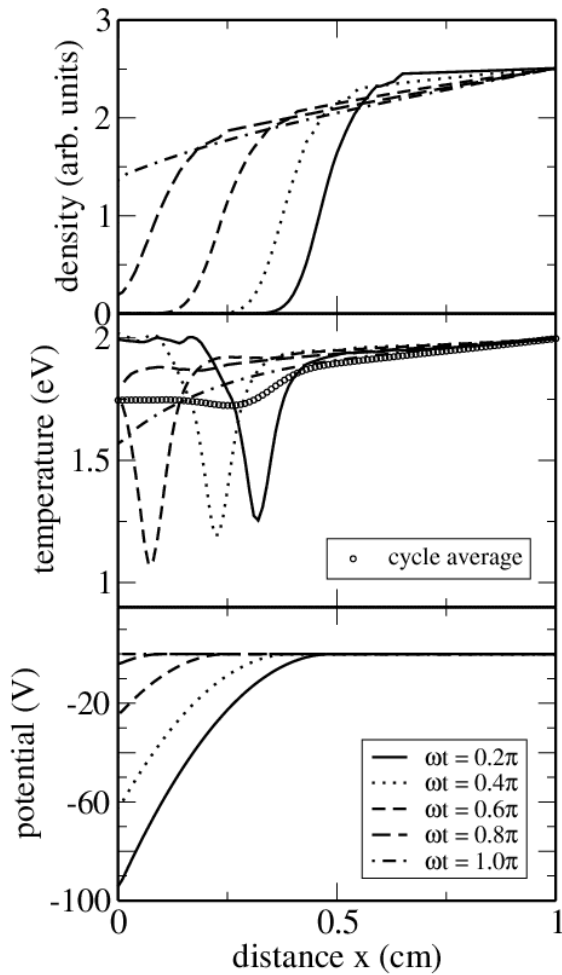
Figure 9. Electron heating by the RF sheath. The term with $\partial\phi/\partial t$ in Eq. (7). is turned off.
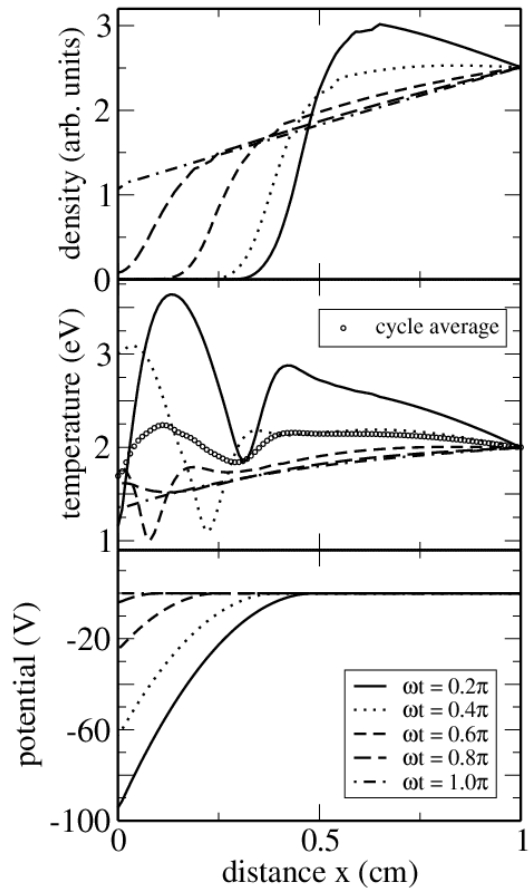

Figure 10. Electron heating by the RF sheath. The term with $\partial\phi/\partial t$ in Eq. (7) is turned on.

The importance of spatial gradients in the kinetic equation is illustrated in Figures 11-14. These figures compare the results of simulations using the local Boltzmann equation with the solution of the non-local equation (7) for a 1D 13.56 MHz CCP discharge at pressures of 100 and 400 mTorr.
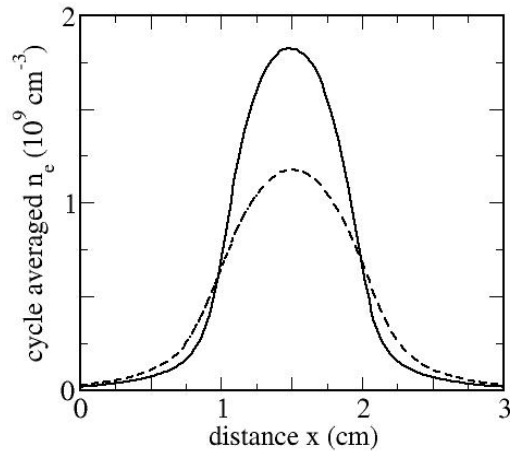

Figure 11. Electron density distribution for CCP at 100 mTorr calculated using non-local model (solid line) and local model (dashed line).

The model reproduces the results of PIC simulations for simple benchmark cases and for more complicated hydrocarbon plasma simulations (see Ref. 37). It could be applied to multi-dimensional simulations of industrial multi-frequency CCP reactors used in modern semiconductor manufacturing.

C. Positive Column

Positive column of DC discharges is a classical object of gas discharge physics [65] having important applications for light sources [66] and gas lasers. Kinetic models based on Monte Carlo simulations and solutions of Boltzmann equation for electrons have been frequently used in studies of positive column (see, for instance [67,68,69,70,71,72] and references therein). Below, we illustrate some results of recent simulations of positive column of rare gases performed for a wide range of discharge parameters (gas pressures 0.1-100 Torr, and currents μA-0.1 A). [73]

For simulation of positive column of DC discharges, the radial electrostatic potential can be included in the total energy and the axial electric field E_z regarded as an electron heating source described by the diffusion coefficient in energy

$$D_E = E_z^2 D_r \qquad (14)$$

Using a self-consistent model of plasma including non-local Boltzmann solver and Poisson solver, we have simulated the positive column plasma for a wide range of pressures (0.1-100 Torr) and currents (mA-0.1A) in Ar and He gases. The axial electric field E_z was found self-consistently for a given discharge current I. Figure 15a shows the dependence of E_z on discharge current and power in Argon for $pR = 100$ Torr cm. Figure 15b shows results of similar calculations for Neon [9] using different physical models. The observed hysteresis is due to current constriction described below.
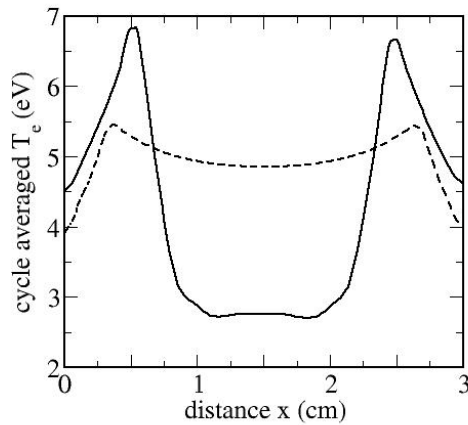

Figure 12. Electron temperature distribution for CCP at 100 mTorr calculated using non-local model (solid line) and local model (dashed line).
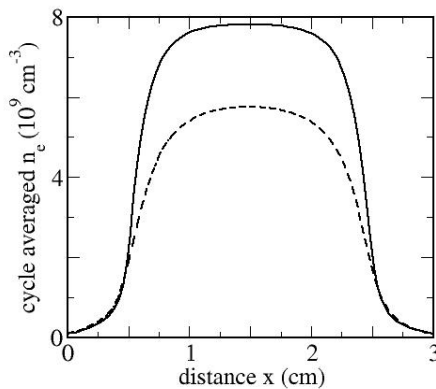

Figure 13. Electron density distribution for CCP at 400 mTorr calculated using non-local model (solid line) and local model (dashed line).
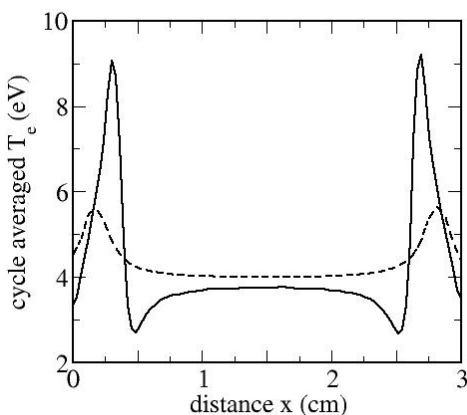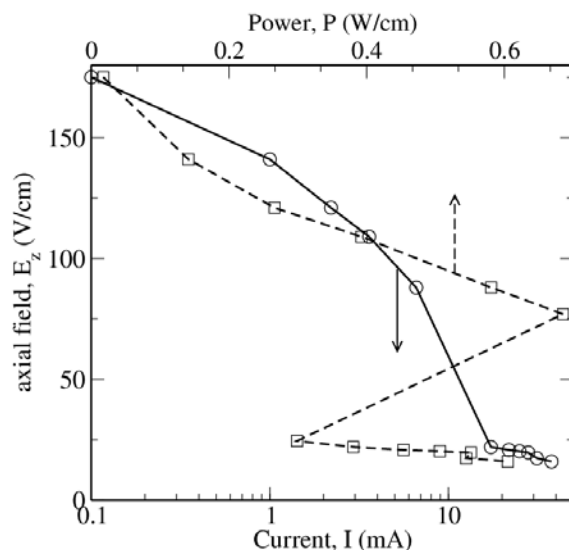

Figure 14. Electron temperature distribution for CCP at 400 mTorr calculated using non-local model (solid line) and local model (dashed line).
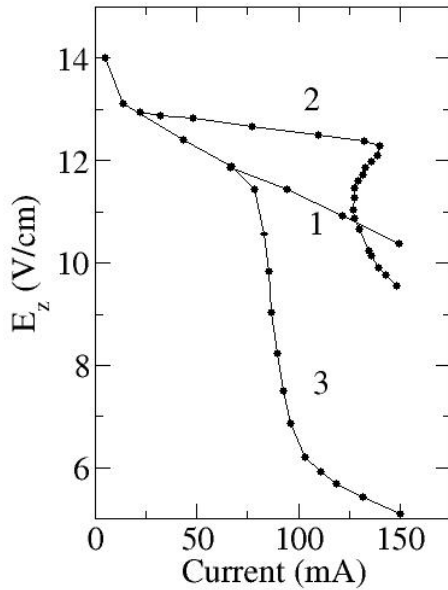
Figure 15. a) Axial electric field E_z in argon PC as function of discharge current and absorbed power for pR = 100 Torr cm; b) same for neon at pR=96 Torr cm [9], curve 1 with account for gas heating and neglect of Coulomb collisions, 2 – with neglect of gas heating, 3- with account for both factors.

An interesting phenomenon was discovered in these simulations at moderate pressures in Argon. The model included 6 plasma species [74]: Ar (ground state), Ar* and Ar** (two metastable states with energies u^* = 11.55 eV and u^{**} = 13.2 eV, correspondingly), Ar$_r^*$ (resonance state), Ar$^+$ and Ar$_2^+$ (atomic and molecular ions). The chemistry mechanism similar to [75] consisted of 21 reactions including conversion of atomic to molecular ions, various electron-induced excitation and ionization steps, radiation transitions from Ar** to Ar* states (rate constant 3×10^7 s^{-1}) and from Ar$_r^*$ to Ar. Radiation trapping was calculated according to [76], with accounts for both Doppler and collisional line broadening. At pressures in the range of $5 < p < 50$ Torr and low discharge currents of the order of 1 mA, non-monotonic radial distributions of excitation rates and metastable density profiles have been observed [77]. This surprising effect, first observed in the numerical simulations (see Fig. 16), later found a theoretical interpretation in [78] based on specifics of nonlocal electron kinetics.
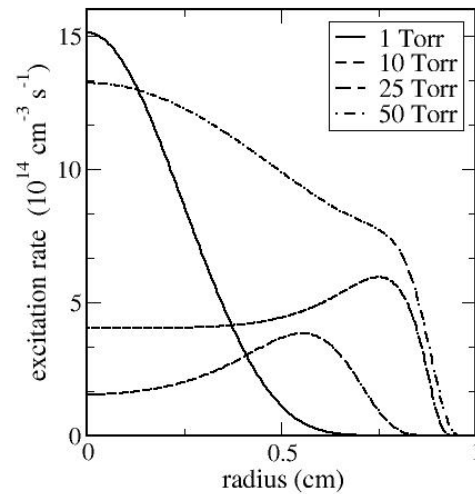
Figure 16. Radial distribution of electron density in positive column of radius R= 1 cm for discharge current I = 1 mA.

At high pressures, the current constriction towards the discharge axis was observed in simulations with an increasing discharge current (see Fig 15). The current constriction takes place at about 10 mA discharge current and is accompanied by the formation of a narrow current channel near the axis (see Figure 17). The width of the channel is determined by the volume recombination [79]. When this width becomes comparable to the energy relaxation length, non-local effects become important, as illustrated in Figure 18.

Figure 17. Radial distribution of charged particle densities and gas temperature in the constricted positive column of radius R= 1 cm for discharge current I = 25 mA.

Figure 18. Radial distributions of electron temperature and electrostatic potential in the constricted positive column for dis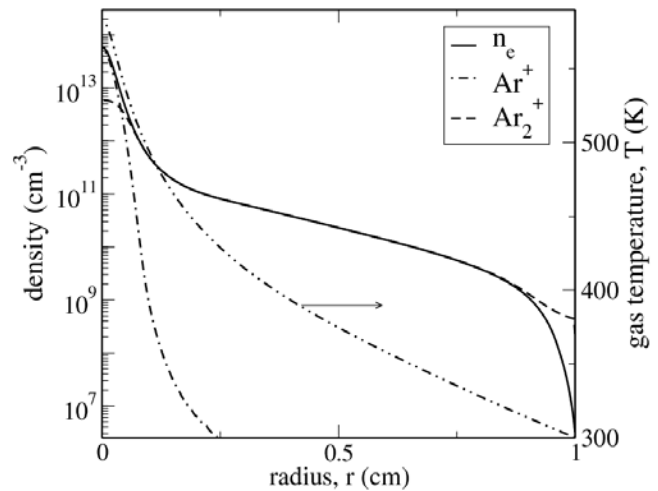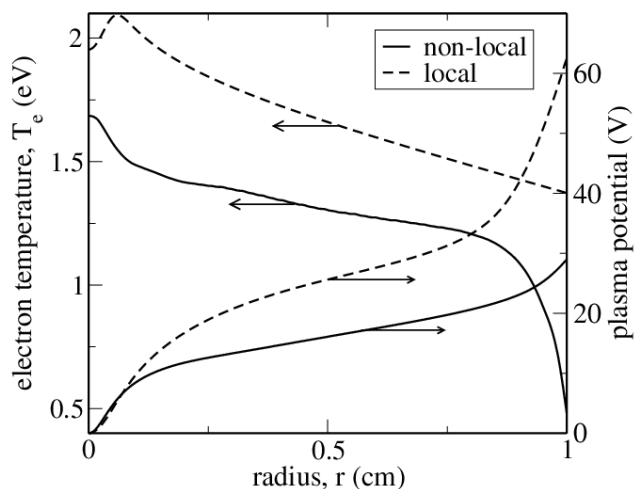charge current $I = 25$ mA: solid lines show results of the non-local model and the dashed lines those of the local model.

As discussed in detail in [80],[9], gas heating plays an important but not decisive role during PC constriction in rare gases, except Helium. The main effect is caused by the non-linear dependence of atomic excitation rate on electron density caused by the Maxwellization of the EEPF due to Coulomb interactions among electrons (see below). In Helium, the constriction occurs in the form of an "optical constriction", i.e. localization of excitation rates towards the axis (see Ref 9 for more details). Figure 15b illustrates the effects of different factors on the current-voltage characteristics of PC in Neon.

D. Striations

Standing and/or moving striations in the positive column of DC discharges have been studied for over a century. Striations were observed in a wide range of pressures (10^{-3}-10^{3} Torr) and currents (10^{-4}-10 A) in almost all gases. Standing striations are seen by the naked eye in molecular gases (H_2, N_2, and mixtures of molecular and rare gases). Moving striations (in rare gases) are more difficult to observe due to their high velocity (10-1000 m/s) and frequency (1-1000 kHz). Dispersion characteristics of striations are rather interesting and different for different types of striations. The phase velocity (ω/k) is usually directed from anode to cathode, the group velocity ($d\omega/dk$) can be either directed towards the cathode (direct waves) or towards the anode (reverse waves). Several types of striations have been identified in rare gases depending on gas pressure and discharge currents. Latest reviews can be found in [81,9,10].

Moving striations have been obtained in computer simulations in Argon at low gas pressure and high discharge current [82] (near the so-called Pupp limit). The procedure of simulation was the following. First, a spatially homogeneous kinetic equation for EEPF (7) was solved with account of

Coulomb collisions for a range of E/N and n_e and Look Up Tables (LUT) were created for the transport coefficients and ionization rates as functions of mean kinetic energy $\langle u \rangle$ and electron density n_e. The EEPF Maxwellization due to Coulomb collisions among electrons results in a strong dependence of inelastic collision rates on electron density (Fig. 19). This effect is most pronounced for the elastic energy balance of electrons (low E/N). Figure 20 shows an example of LUT for the electron temperature $T_e = 2\langle u \rangle/3$ as a function of reduced electric field E/p and electron density.
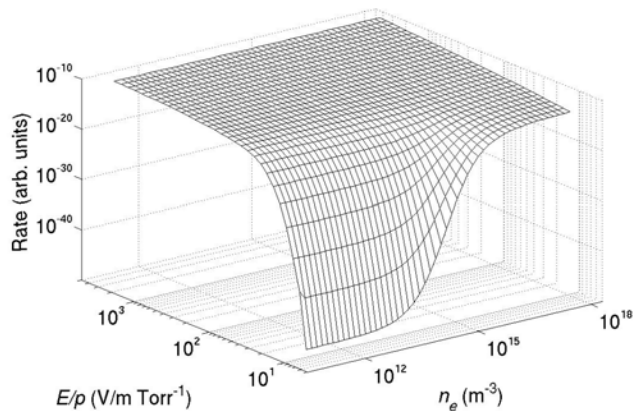
Figure 19. Rate of inelastic collisions as a function of electric field and electron density.
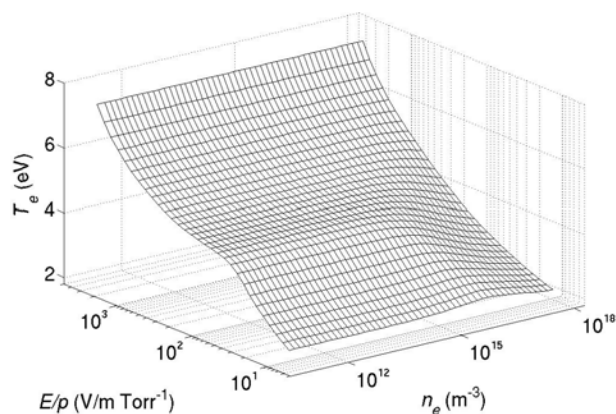
Figure 20. Electron temperature as a function of electric field and electron density.

Having obtained the LUTs, continuum equations for electron density and mean kinetic energy were solved together with the Poisson equation using the electron transport coefficients and reaction rates from the LUTs. The boundary conditions for electrons at the cathode were defined taking into account either thermal or secondary emission. An external RC circuit was also used similar to [83]. The ion transport was calculated using a fluid model with drift-diffusion approximation for the ion flux.

In such a way, moving striations have been obtained in simulations for one- and two-dimensional settings. The computations reproduced all the main features of striations in Argon PC observed at low pressures and high currents (near the Pupp limit). The computational model could simulate nonlinear waves, near-electrode phenomena and external circuit effects on the striation behavior.

Figure 21 shows an example of 2D simulations for Argon pressure 2 Torr, the discharge current 100 mA, cylindrical tube of length $L = 20$ cm and radius $R = 1$ cm, planar cathode on the left ($x = 0$) and a planar anode on the right ($x = L$). The tube wall (at $r = R$) is assumed to be dielectric; its (local) potential is calculated by time integrating fluxes of electrons and ions to the wall surface. The simulation runs about 30 hours on a 1 GHz desktop computer.
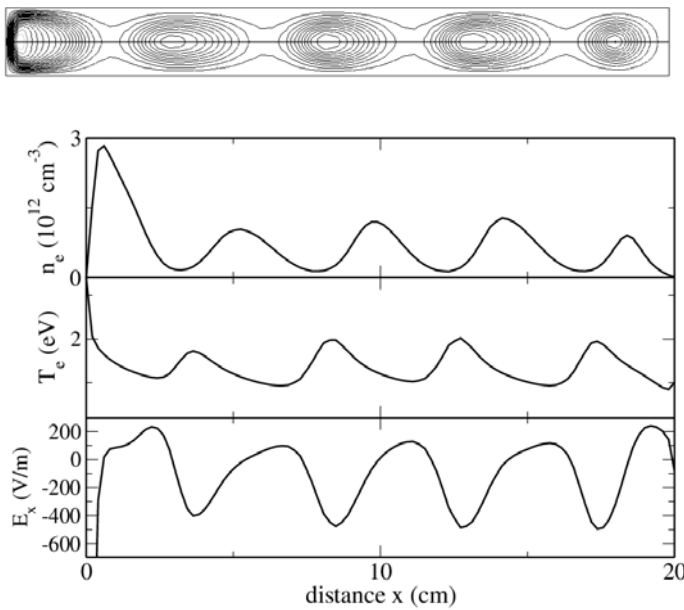

Figure 21. Two-dimensional distribution of plasma density (each contour line corresponds to density variation of about 10^{11} cm^{-3}) and axial distributions of electron density, electron temperature and axial electric field in striations at $p = 2$ Torr and $I = 100$ mA.

It is seen in Figure 21 that the electron temperature is shifted towards the cathode with respect to electron density. This shift is responsible for the shift of ionization rate and the motion of the striations towards the cathode. It is also seen that the electric field changes sign along the striations. This electric field reversal results in trapping of slow electrons in the potential well. At high currents, the trapping does not lead to dramatic consequences since Coulomb collisions provide effective energy exchange between trapped and free electrons.
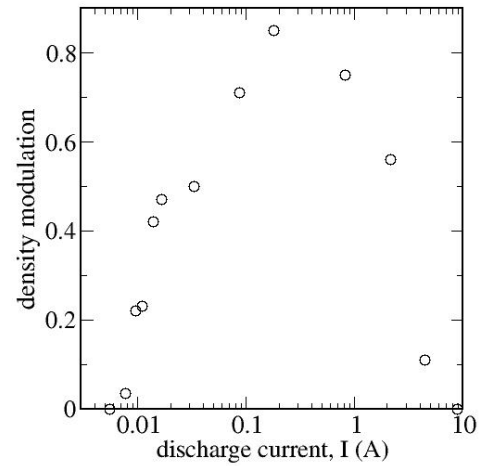

Figure 22. Electron density modulation amplitude versus discharge current in Argon at $p = 1$ Torr.

Figure 22 shows the results of a scan over the discharge current for these conditions: the density modulation amplitude is shown as a function of discharge current. One can see in Figure 22 that at low currents, the discharge is striation-free due to low electron density values (and high electric fields) and the absence of nonlinearity of the ionization rate with electron density. The discharge is striation-free at high currents as well due to large electron densities and the resulting saturation of the ionization rate with electron density. The discharge parameters are strongly modulated at currents between several 10 mA's and several A's, as seen in Figure 22. These results are in agreement with experimental observations near the Pupp limit.

No self-consistent simulation of kinetic striations observed at low currents has been reported so far. Electron kinetics in spatially uniform and spatially periodic striation-like fields have been extensively studied by Golubovskii and Winkler groups (see Refs [84], [11] and references therein). The numerical experiments confirmed the resonance character of electron interaction with spatially periodic fields predicted by analytical models [85,86,87] and previously simulated by Shveigert [88]. Recently, a new resonance has been uncovered for large modulation of the field and attributed to R striations observed in experiments (see Ref. 84).

Figure 1 can be used to illustrate typical features of the EEPF formation in a spatially modulated static electric field. The electrons are injected from the left boundary, $x=0$, and accelerated by the electric field

$$E(x) = E_0 \left(1 + \alpha \sin\left(\frac{2\pi x}{L} \right) \right) \qquad (15)$$

The field amplitude E_0 and modulation depth α can be varied in these simulations. The spatial relaxation of the EEPF in rare gases occurs due to energy loss in elastic collisions, excitation of several atomic levels with different

energy quantum and Coulomb interactions among electrons [88],[89]. Near the boundary, damping oscillations are formed with a spatial period, L_S, corresponding to the averaged value of the electric field, $L_S = U_s / E_0$. Here $U_s = U_1 + \Delta U$, U_1 is the first excitation potential and $\Delta U < U_1$ depends on specifics of the relaxation process. Far from the boundary, the period of oscillations is determined by the period of the field L and the amplitude of oscillations has resonance character (see Fig. 23).
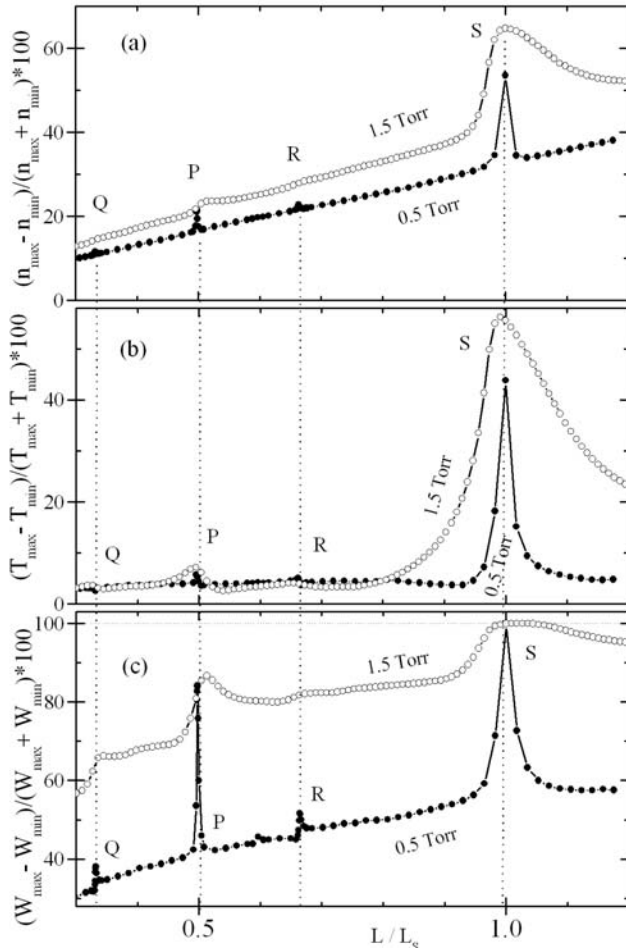

Figure 23. Modulation amplitude of electron density (a), electron temperature (b) and excitation rate (c) as function of the field period L / L_S for $\alpha = 0.9$ (from Ref. 84).

The maximum modulation of electron density n_e, electron temperature T_e, and excitation rate W occurs at $L = L_S, L_S / 2, L_S / 3$ and $L = 2 L_S / 3$. The first type of resonance was predicted by the linear theory (see Ref 85), the second type was observed in [84] only for substantial modulation of the electric field. The $L = L_S$ resonance corresponds to S striations, the $L_S / 2$ resonance corresponds

to P striations, and the $L = 2 L_S / 3$ resonance was attributed to R striations observed in experiments.

E. Effect of Static Magnetic Field

In the presence of a static magnetic field, the spatial diffusion coefficient D_r in the kinetic equation (7) becomes a tensor. The D_r component along the magnetic field is not affected by the field, the component orthogonal to the field is suppressed. When the magnetic field is orthogonal to the electric field, its effect can be described in terms of the effective collision frequency

$$v_{eff} = v(1 + (\omega_B / v)^2) \qquad (16)$$

where ω_B is the electron cyclotron frequency and is equivalent to an increase in gas pressure. This effect explains the impact of magnetic fields on spatial relaxation of electrons [90] and specifics of electron kinetics in magnetron discharges between coaxial electrodes [91].

More interesting phenomena take place in a positive column submerged in an axial magnetic field. The electric field in the positive column has both axial and radial components. The radial diffusion of the electrons is suppressed by the axial magnetic field, $D_r = v^2 / (3 v_{eff})$, whereas the electron heating described by the energy diffusion D_E remains unchanged. As a result, the increase of the magnetic field is accompanied by the transition from nonlocal to local mode and exhibits a maximum of the axial electric field sustaining the plasma [92].

IV. COLLISIONLESS EFFECTS

A number of interesting phenomena have been observed in the near-collisionless regime, when the electron mean free path is comparable or larger than discharge dimensions, In classical DC discharges, among these phenomena are the Langmuir paradox [93], ion-sound and ionization waves [94], etc. In RF discharges, the well known are stochastic electron heating and anomalous skin effect. Classical works on the anomalous skin effect in bounded plasmas were reviewed by Kolobov [95],[96]. Recently, collisionless effects in inductively coupled plasmas have been studied in a series of experimental papers by Godyak et al (see [7] and references therein), and theoretical papers by Turner [97], Vahedi et al. [98], Cohen and Rognlien [99], Shaing [100], Yoon et al. [101],[102],[103],[104], Seo et al. [105], Tushetsky et al. [106], Kaganovich et al. [107],[108],[109],[110],[111] and references therein). Results of these studies are partially reflected in the second edition of the book [8]. Stochastic electron heating and anomalous skin effect observed in radio frequency discharges at low gas pressures are of practical importance for plasma reactors currently used for

semiconductor manufacturing.

When the electron mean free path is comparable or larger than discharge dimensions, the EEPF of trapped electrons depends solely on total electron energy. Solutions of spatially inhomogeneous kinetic equation (7) confirm this statement with high accuracy (see Figure 24). In this regime, electron collisions with plasma boundaries dominate over collisions with atoms. Strictly speaking, the two-term SHE is not valid under these conditions, and the EEPF can be found from a kinetic equation averaged over the discharge volume [107],[112]. The energy diffusion coefficient and the heating rate are determined by integration over electron trajectories.
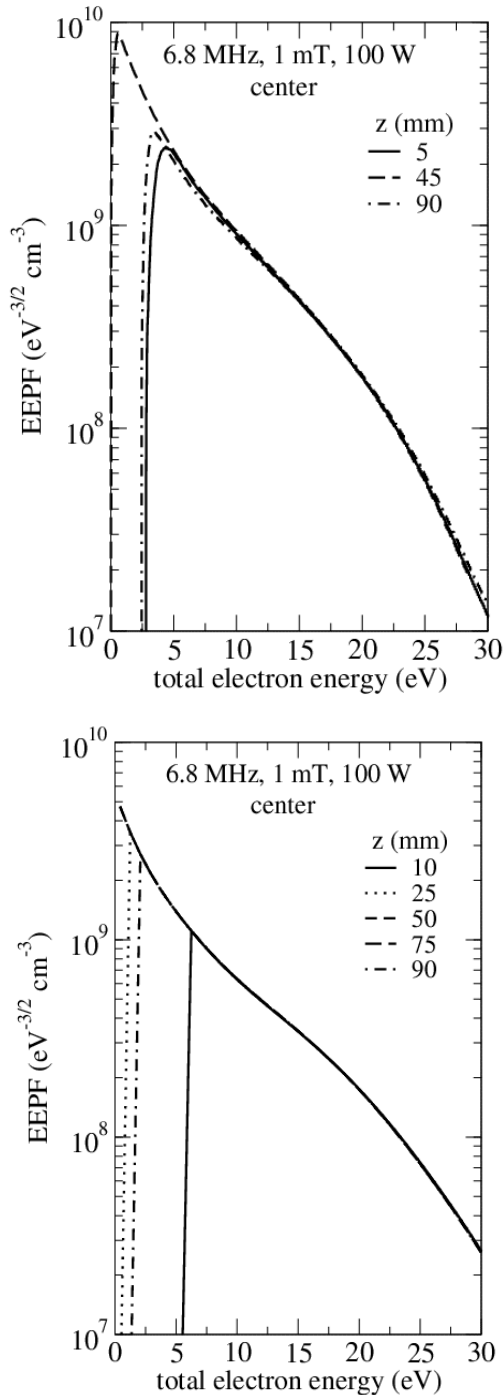

Figure 24. Experimental (a) and calculated (b) EEPFs in Argon ICP at different points along the discharge axis at $r=0$ (from Ref. 46).

Until recently, mostly analytical models and PIC simulations have been used for studies of collisionless effects in gas discharge plasmas. Stochastic electron heating was commonly observed in PIC simulations of CCP (see Ref. 8) Some of the collisionless effects have been observed in ICP simulations using Monte Carlo models for electron kinetics [113],[45].

Vlasov solvers developed for the collisionless plasma can be adapted to studies of low-pressure gas discharges. Figure 25 shows results obtained with our 6D Vlasov solver for electron acceleration by an oscillating RF sheath. In these simulations, the electric field was specified in the form

$$E(x,t) = \begin{cases} A(x-s) , & 0 < x < s(t) \\ 0 & L > x > s(t) \end{cases} \quad (17)$$

where $s(t) = s_0 + s_1 \cos(\omega t)$. Electrons are injected from one (right) side with a given distribution function (half-Gaussian with normalized density $\tilde{n}_e = 1$ and temperature $\tilde{T}_e = 1$). The electron velocity is normalized to thermal velocity v_{th}, the characteristic frequency of the system is $\omega_0 = v_{th}/L$. Figure 25 shows the temporal behavior of the distribution function at the sheath edge $s = s_0 + s_1$ for two driving frequencies, $\omega/\omega_0 = 0.01$ and 1. One can see that the distribution function of electrons moving out of the sheath ($V_x > 0$) is strongly modulated at $\omega/\omega_0 = 0.01$ and only slightly modulated at $\omega/\omega_0 = 1$. At low frequencies, electrons are being accelerated by the moving sheath boundary and at high frequencies they do not respond to the field oscillations. It should be noted that electron plasma frequency does not appear in this analysis since Poisson equation is not solved and the field profile is prescribed *a priory* by Eq. (17).
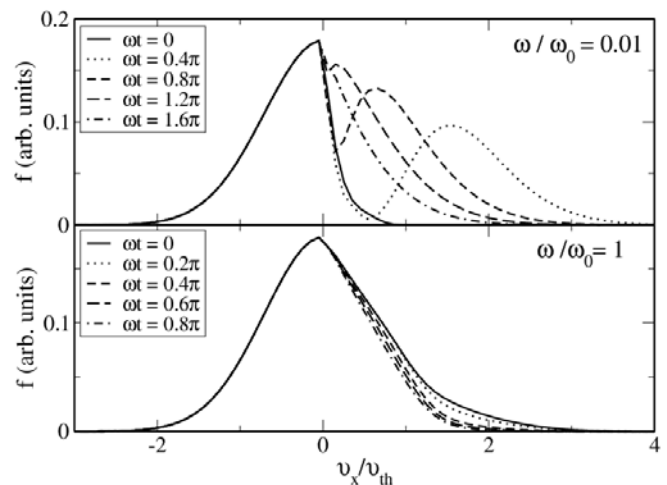
Figure 25. Distribution function f versus V_x-velocity at the sheath edge for two RF frequencies. f is shown at 5 times for a full cycle at $\omega = 0.01$ and for a half-cycle at $\omega = 1$.

Among a variety of hot plasma effects observed in ICP [114] are non-monotonic distributions of electric and magnetic fields, generation of electrostatic potential perturbation in the skin layer, collisionless electron heating etc. Figure 26 shows an example of recent simulation of these effects using a Vlasov solver [115].
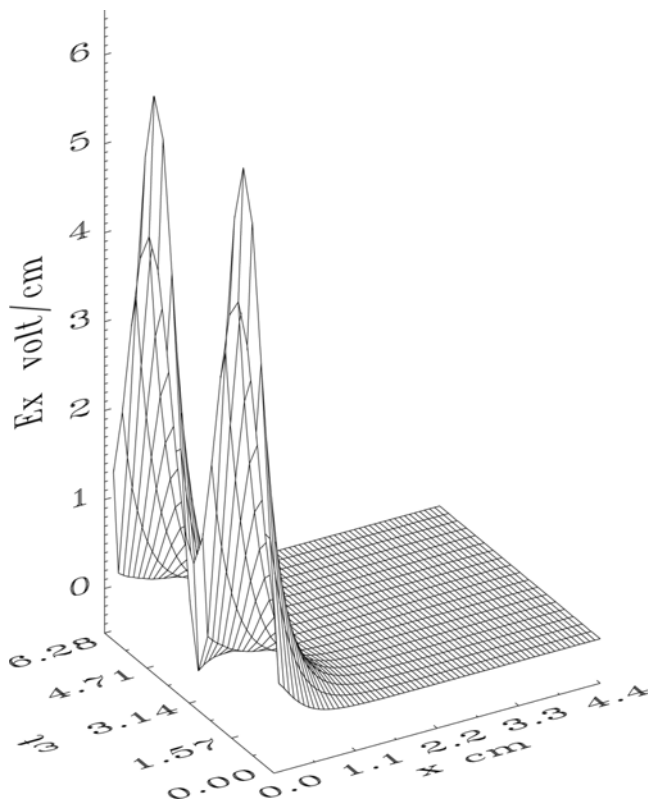

Figure 26. Longitudinal electric field in the skin layer (from Ref. 115)

In Ref. [115], a set of Vlasov equations for electrons and ions was solved together with Maxwell equations for the electric field E_y and magnetic field B_z and Poisson equation for the electric field E_x in a one-dimensional case, for the wave frequencies 13.56 and 6.78 MHz. The results of analytical model [99] were confirmed in these simulations. The fields, E_y and B_z decay exponentially from the plasma boundary at $x=0$, within the skin layer. Owing to large difference of electron and ion mass, an electrostatic field is created in the skin layer by the Lorentz forces at the second harmonic of the applied electric field (see Figure 26). Since the skin depth is much larger than Debye length and the wave frequency is much smaller than electron plasma frequency, the plasma remains quasi-neutral in the skin layer. Solving Poisson equation requires a high accuracy under these conditions since small charge separation of the order of 10^{-4} creates noticeable fields in the plasma. The use of low noise Vlasov code is crucial in this case because the noise level of particle codes cannot allow required accuracy.

V. CONCLUSION

Numerous phenomena in gas discharge physics cannot be properly understood without kinetic analysis of electrons. We have reviewed the recent progress in the numerical solution of the Boltzmann equation for simulation of electron kinetics in gas discharge plasmas. The reduction of the 6D Boltzmann equation to a 4D Fokker Planck equation using two-term spherical harmonics expansion enables efficient and accurate simulation of the electron distribution function in collisional gas discharge plasmas. This approach has also been successfully used for simulation of electron transport in semiconductor devices [116],[117] and collisionless electron transport in plasma thrusters [118]. It covers a niche between the particle simulation methods and semi-analytical discharge models. The two-term approximation, called diffusion approximation in mathematical literature, works unexpectedly well even beyond its range of validity.

Simulations of weakly-collisional plasmas have been traditionally performed by Particle-in-Cell (PIC) codes. Recently, Vlasov codes have been also applied to simulations of collisionless effects in gas discharges. We believe, with further development of the numerical methods and computing power, these methods will offer a viable alternative to statistical methods for certain classes of problems. Among promising methods for increasing efficiency of the deterministic kinetic solvers is adaptive mesh refinement in phase space [119]. The adaptive mesh refinement technologies have already been used with fluid discharge models [120] and are being actively developed now for simulation of streamer discharges.

VI. ACKNOWLEDGMENT

Vladimir I. Kolobov (M'00–SM'03) was born in Novgorod region, USSR, in 1960. He received the M.S. and Ph.D. degrees in physics from the Leningrad State University in 1984 and 1989, respectively.

He was a Visiting Scientist in the Laboratoire des Discharges dans les Gaz, Universite P. Sabatier, in Toulouse, France in 1992-93, in the Engineering Research Center for Plasma-Aided Manufacturing at the University of Wisconsin in Madison in 1994-95, and in the Plasma Processing Laboratory at the University of Houston in 1995-97. Dr. Kolobov joined CFD Research Corporation In Huntsville, AL in October 1997 and has been

responsible for the development of plasma technologies and commercial software for plasma simulations. He is an expert in the kinetic theory and computational physics, the author of over 50 journal articles and numerous conference presentations..

Dr. Kolobov is a member of AIAA and a member of the Executive Committee of the Plasma Science and Applications Committee of the IEEE Nuclear and Plasma Sciences Society.

Robert R. Arslanbekov PhD, Principal Scientist at CFDRC

REFERENCES

[1] U.Kortshagen and L.D.Tsendin, Eds, *Electron Kinetics and Applications of Glow Discharges*, Plenum Press, New York, 1998

[2] V.I.Kolobov and V.A. Godyak, "Non-Local Electron Kinetics in Collisional Gas Discharge Plasmas", IEEE Transactions on Plasma Science **23**, 503 (1995)

[3] G.E.Geoghiou, A.P.Papadakis, R.Morrow and A.C Metaxas, Numerical modeling of atmospheric pressure gas discharges leading to plasma production, J. Phys. D. **38**, R303 (2005)

[4] R.E.Robson, R.D.White, Z.Lj.Petrovic, Colloquium: Physically based fluid modeling of collisionally dominated low-temperature plasmas, Rev. Mod. Phys. **77**, 1303 (2005)

[5] G.J.M.Hagelaar and L.C.Pitchford, Solving the Boltzmann equation to obtain electron transport coefficients and rate coefficients for fluid models, Plasma Sources Sci. Technol. 14, 722 (2005)

[6] L.D.Tsendin, Electron kinetics in non-uniform glow discharge plasmas, Plasma Source Sci. Technol. **4**, 200 (1995).

[7] V.Godyak, Hot plasma effects in gas discharge plasma, Phys. Plasmas **12**, 055501 (2005)

[8] M.A.Liberman and A.J. Lichtenberg, *Principles of plasma discharges and material's processing*, Second Edition, Wiley, 2005

[9] Yu.B.Golubovskii, A.A.Kudryavtsev, V.O.Nekuchaev, I.A.Porokhova, and L.D.Tsendin, *Electron kinetics in non-equilibrium gas discharge plasmas*, St. Petersburg University Press, 248p (2004) (in Russian)

[10] V.E.Fortov, Ed, *Encyclopedia of Low Temperature Plasmas*, Moscow, Nauka, (2000), in 4 volumes (in Russian)

[11] R.Winkler et al, Progress of the Electron Kinetics in Spatial and Spatiotemporal Plasma Structures, Contrib. Plasma Phys. **44**, 437 (2004)

[12] H.C.Kim. F.Iza, S.S.Yang, M.Radmilovic-Radjenovic, and J.K.Lee, Particle and fluid siulations of low temperature plasma discharges: benchmark and kinetic effects, J. Phys. D **38**, R283 (2005)

[13] A.Bogaerts, K. de Bleecker, I.Kolev, M.Madani, Modeling of gas discharge plasmas: What can we learn from it?, Surface and coatings technology **200**, 62 (2005)

[14] J.P.Verboncoeur, Particle simulation of plasmas: review and advances, Plasma Phys. Control. Fusion **47**, A231 (2005)

[15] M.Shiozawa and K.Nanbu, Coupling of plasma and flow in materials processing, Thin Solid Films **457**, 48 (2004)

[16] C. Cercignani, *The Boltzmann Equation and its Applications*, Springer-Verlag, (1988).

[17] E M Lifshitz, L P Pitaevsky, *Course of Theoretical Physics: Vol. 10 Physical Kinetics*, Pergamon Press (1981)

[18] P.P.J.M.Schram, *Kinetic theory of gases and plasmas*, Kluwer Academic Publishers, 1991

[19] V.P.Vstovsii, Kinetics of a weakly ionized plasma in external field, Sov. J. Plasma Phys. **12**, 856 (1986)

[20] I.Shkarofsky, T.Johnston, M.P.Bachinski, *The Particle Kinetic of Plasmas*, Reading: Addison-Wesley, (1981) 452p

[21] U.Kortshagen, C.Busch and L.D.Tsendin, On simplifying approaches to the solution of the Boltzmann equation in spatially inhomogeneous plasmas, Plasma Sources Sci. Tech. **5**, 1 (1996)

[22] RD White, RE Robson, B.Schmidt and MA Morrison, Is the classical two-term approximation of electron kinetic theory satisfactory for swarms and plasmas, J. Phys. D **36**, 3125 (2003)

[23] P. Degond, An infinite system of diffusion equations arising in transport theory: The coupled Spherical Harmonics Expansion model, Mathematical Models and Methods in Applied Science **11**, 903 (2001)

[24] L.M. Biberman, V.S. Vorob'ev, I.T. Yakubov, *Kinetics of Nonequilibrium Low-Temperature Plasmas*, Springer (1987)

[25] E.M.Epperlein, Fokker-Planck modeling of electron transport in laser-produced plasmas, Laser and Particle Beams **12**, 257 (1994)

[26] M.O.M.Mahmoud and M.Yousfi, Boltzmann equation analysis of spatiotemporal swarm development, J. Appl. Phys. **81**, 5935 (1997)

[27] L.D.Tsendin, Electron distribution function of weakly ionized plasmas in nonuniform electric fields.I Weak fields, Sov. J. Plasma Phys. **8**, 96 (1982)

[28] J.R.Albritton, Laser absorption and heat transport by non-Maxwell-Boltzmann electron distribution, Phys. Rev. Lett. **50**, 2078 (1983)

[29] A.Kudryavtsev and L.D.Tsendin, Cathode boundary conditions for fluid models of gas discharges on the righ-hand branch of the Pashen curve, Tech. Phys. Lett. **28**, 621 (2002)

[30] F.Sigeneger and R.Winkler, Response of the Electron inetics on Spatial Disturbances of the electric field in non-isothermal plasmas, Contrib Plasma Phys. **36**, 551 (1996)

[31] H-H.Choe, N.S.Yoon, S.S.Kim and D-I Choi, A new unconditionally stable algorithm for steady-state Fluid simulations of high density plasma discharges, J. Comp. Phys. **170**, 550 (2001)

[32] E.P.Hammond, K.Mahesh and P.Moin, A numerical method to simulate radio-frequency plasma discharges, J. Comp. Phys. **176**, 402 (2002)

[33] V.I.Kolobov, Fokker-Planck modeling of electron kinetics in plasmas and semiconductors, Computational Material Science **28**, 302 (2003)

[34] G.J.M.Hagelaar and G.M.W.Kroesen, Speeding up fluid models for gas discharges by implicit treatment of the electron energy source term, J. Comp. Phys. **159**, 1 (2000)

[35] F.Alouani-Bibi, M.MShoucri, J-P Matte, Different Fokker-Planck approaches to simulate electron transport in plasmas, Comp. Phys. Comm. **164**, 60 (2004)

[36] V.I.Kolobov and R.R.Arslanbekov, Deterministic Boltzmann solver for electron kinetics in plasma reactors for microelectronics applications, Microelectronic Engineering **69**, 606 (2003)

[37] V.I.Kolobov and R.R. Arslanbekov, Four-dimensional Fokker-Planck solver for electron kinetics in collisional gas discharge plasmas, Computer Physics Comm. **164**, 195 (2004)

[38] R.J.Kingham and A.R.Bell, An implicit Vlasov-Fokker-Planck code to model non-local electron transport in 2-D with magnetic fields, J. Comp. Phys. **194**, 1 (2004)

[39] R.Winkler, V.A.Maiorov, F.Sigeneger, Impact of magnetic fields on the spatial relaxation of electrons, J. Appl. Phys. **87**, 2708 (2000)

[40] I.A.Porokhova, Yu.B.Golubovski, et al, Two-dimensional nonlocal model of axially and radially inhomogeneous plasma of cylindrical magnetron discharge, Phys. Rev. E **68**, 016401 (2003)

[41] Z.Lj. Petrovic, Z.M.Raspopovic, S.Dujko and T.Makabe, Kinetic phenomena in electron transport in radio-frequency fields, Appl. Surf. Science **192**, 1 (2002)

[42] E.Pohn, M.Shoucri, G.Kamelander, Eulerian Vlasov codes, Computer Physics Comm. **166**, 81 (2005)

[43] V.A.Godyak, R.B.Piejak and B.M Alexandrovich, Experimental setup and electrical characteristics of an inductively coupled plasma, J. Appl. Phys. **85**, 703 (1999)

[44] V.A.Godyak, R.B.Piejak and B.M.Alexandrovich, Electron energy distribution function measurements and plasma parameters in inductively coupled argon plasma, Plasma Sources Sci. Technol. **11**, 525 (2002)

[45] A.V.Vasenkov and M.J.Kushner, Electron energy distributions and anomalous skin depth effects in high plasma density inductively coupled discharges, Phys. Rev. E **66**, 066411 (2002)

[46] V.I.Kolobov, R.R.Arslanbekov, N.Zhou, V.A.Godyak, Comparison of spatially resolved experimental and calculated electron distribution functions and other plasma parameters in inductively coupled argon plasma, Program

56th Annual Gaseous Electronics Conference, Bull. Am. Phys. Soc. 58(6), p.18, ET26 (2003)

[47] U.Kortshagen, I. Pukropski and L.D.Tsendin, Experimental investigation and fast two-dimensional self-consistent kinetic modeling of a low pressure inductively coupled rf discharge, Phys. Rev. E **51**, 6063 (1995)

[48] G.Mumken, Spatial profiles of a planar inductively coupled discharge in Argon, J. Phys. D **32**, 804 (1999)

[49] U.Kortshagen and B.Heil, Kinetic modeling and experimental studies of large scale low pressure RF discharges, J. Tech. Phys. **41**, 325 (2000)

[50] R.Piejak, V.Godyak, B.Alexandrovich, N.Tishchenko, Plasma Sources Science Technol. **7**, 590 (1998)

[51] M.W.Kiehlbauch and D.B.Graves, Modeling argon inductively coupled plasmas, J. Appl. Phys. **91**, 3539 (2002)

[52] V.E.Golant, A.P.Zhilinskii, I. E. Sakharov, *Fundamentals of Plasma Physics*, John Wiley & Sons Inc (1980)

[53] S.Djurovic, J.R.Roberts, M.A.Sobolevski and J.K.Olthoff, Absolute spatially and temporally resolved optical emission mesurements of rf glow discharges in argon, J. Res. NIST **98**, 159 (1993)

[54] U.Czarnetski and VA Kadetov, Optical time modulation spectroscopy, Proc. XXVI ICPIG, Greifswald, Germany (2003)

[55] A.Mareska, K.Orlov and U.Kortshagen, Experimental study of diffusive cooling of electrons in a pulsed inductively coupled plasma, Phys. Rev. E **60**, 056405 (2002)

[56] V.A.Godyak and B.M.Alexandrovich, Plasma parameter evolution in a periodically pulsed ICP, Proc. XXVII ICPIG, Report 06-930, Eindhoven, Neitherlands (2005)

[57] V.I.Demidov, C.A. DeJoseph, Jr, and A.A.Kudryavtsev, Anomalously high near-wall sheath potential drop in a plasma with nonlocal fast electrons, Phys. Rev. Lett. **95**, 215002 (2005)

[58] V.A.Godyak, *Soviet Radio Frequency Discharge Research*, Delphic Ass. Inc. Falls Church, VA (1986)

[59] Yu.P.Raizer, M.N.Shneider, N.A.Yatsenko, *Radio-Frequency Capacitive Discharges*, CRC Press, 1995.

[60] G.Gozadinos, M.M.Turner and D.Vender, Collisionless electron heating by capacitive RF sheaths, Phys. Rev. Lett. **87**, 135004 (2001)

[61] G.Chen and L.Raja, Fluid modeling of electron heating in low-pressure, high-frequency capacitively coupled plasma discharges, J. Appl. Phys. **96**, 6073 (2004)

[62] N.Xiang, Effects of electron inertia in capacitively coupled radio-frequency discharges, Phys. Plasmas **11**, 4213 (2004)

[63] A.A.Howling et al., Probe measurements of plasma potential nonuniformity due to edge assymmetry in large area radio-frequency reeactors: the telegraph effect, J. Appl. Phys **97**, 123308 (2005)

[64] P.Chabert et al, Inductive heating and E to H transition in capacitive discharges, Phys. Rev. Lett. **95**, 205001 (2005)

[65] Yu.P.Raizer, *Gas discharge Physics*, Springer, 1991

[66] G.G.Lister, J.E.Lawler, W.P.Lapatovich and V.A.Godyak, The physics of discharge lamps, Rev. Mod. Phys. **76**, 541 (2004)

[67] J.E.Lawler and U.Kortshagen, Self-consistent Monte Carlo simulations of the positive column of gas discharges, J. Phys. D **32**, 3188 (1999)

[68] E.Kawamura and J.H.Ingold, Particle in cell simulations of low pressure small adius positive column discharges, J. Phys. D **34**, 3150 (2001)

[69] L.L.Alves, G.Gousset and C.M.Ferreira, Self-consistent solution to the spatially inhomogeneous electron Boltzmann equation in a cylindrical plasma positive column, Phys. Rev. E **55**, 890 (1997)

[70] Yu.B.Golubovskii, I.A.Porokhova, J.Behnke, J.F.Behnke, A comparison of kinetic and fluid models of the positive column of discharges in inert gases, J. Phys. D. **32**, 456 (1999)

[71] JL Guiliani, GM Petrov, JP Apruzese, and J.Davied, Non-local radiation transport via coupling constants for the radially inhomogeneous Hg-Ar positive column, Plasma Sources Sci. Tech. **14**, 236 (2005)

[72] G.Mumken, H.Schluter and L.D.Tsendin, Formation mechanisms of radial electron fluxes in a positive column, Phys, Rev E **60**, 2250 (1999)

[73] R.R.Arslanbekov, V.I.Kolobov, E.A.Bogdanov, and A.A.Kudryavtsev, Simulations of plasmas of positive column in rare gases, The 31th IEEE International Conference on Plasma Science, IEEE Conf. Records –Abstracts 3P46, 249 (2004)

[74] W. J. M. Brok, J. van Dijk, M. D. Bowden, J. J. A. M. van der Mullen and G. M. W. Kroesen, A model study of propagation of the first ionization wave during breakdown in a straight tube containing argon, J. Phys. D. **36**, 1967 (2003).

[75] G. M. Petrov and C. M. Ferreira, Numerical modeling of the constriction of the dc positive column in rare gases, Phys. Rev. E **59**, 3571 (1999).

[76] A. Bogaerts, R. Gijbels, and J. Vlcek, Collisional-radiative model for an argon glow discharge, J. Appl. Phys. **84**, 121 (1998).

[77] R.R.Arslanbekov, V.I.Kolobov, E.A.Bogdanov, A.A.Kudryavtsev, Nonmonotonic excitation rates in argon positive column, Appl. Phys. Letters **85**, 3396 (2004)

[78] L.D.Tsendin, E.A.Bogdanov, A.A.Kudryavtsev, Paradoxical nonmonotonic behavior of excitation-rate spatial profiles in bounded plasmas, Phys. Rev. Letters 94, 015001 (2005)

[79] Yu.B.Golubovskii, V.I.Kolobov and L.D.Tsendin, Two-dimensional theory of ionization waves in a contracted discharge in an inert gas, Sov. Phys. Tech. Phys. 31, 31 (1986)

[80] Yu.B.Golubovskii, V.O.Nekuchaev and E.B.Pelyukhova, Bifurcation analysis of contraction in inert gases, Tech. Phys. 41, 1011 (196)

[81] P.S.Landa, N.A.Miskinova and Yu.V.Ponomarev, Ionization waves in low temperature plasmas, Sov. Phys. Usp. 23, 813 (1980)

[82] R.R.Arslanbekov and V.I.Kolobov, 2-D Simulations of striations in direct current glow discharges in argon, IEEE Trans. Plasma Sci. 33, 354 (2005)

[83] R.R.Arslanbekov and V.I. Kolobov, Two-dimensional simulations of the transition from Townsend to glow discharge and subnormal oscillations, J. Phys. D. **36**, 2986 (2003)

[84] Yu.B.Golubovskii et al, Kinetic resonances and stratification of the positive column of a discharge, Phys. Rev. E **72**, 026414 (2005)

[85] T.Ruzicka and K.Rohlena, On non-hydrodynamic properties of the electon gas in the plasma of a DC discharge, Czech. J. Appl. Phys. B **22**, 906 (1972)

[86] L.D.Tsendin, Electron distribution function of weakly ionized plasmas in nonuniform electric fields.II Strong fields, Sov. J. Plasma Phys. **8**, 228 (1982)

[87] L.D.Tsendin, Ionization kinetics and ionization waves in neon, Sov. Phys. Tech. Phys. **27**, 407 (1982)

[88] V.A.Shweigert, Electron distribution function in inert gas in slightly modulated static electric field, Sov. J. Plasma Phys **15**, 714 (1989)

[89] D.Loffhagen, Impact of electron-electron collisions on the spatial electron relaxation in non-isothermal plasmas, Plasma Chem. Plasma Proc. **25**, 519 (2005)

[90] R.Winkler, V.A.Maiorov, and F.Sigeneger, Impact of magnetic fields on the spatial relaxation of electrons, J. Appl. Phys. **87**, 2708 (2000)

[91] I.A.Porokhova, Yu.B.Golubovski, et al, Kinetic simulation model of magnetron discharges, Phys. Rev. E **63**, 056406 (2001)

[92] D.Loffhagen, S.Arndt, F.Sigeneger et al., Electron kinetics and self-consistent description of inhomogeneous and nonstationary plasmas, Contrib. Plasma Phys. **45**, 309 (2005)

[93] L.D.Tsendin, Current trends in electron kinetics of gas discharges, Plasma Sources Sci. Techol. **12**, S51 (2003)

[94] D.W.Swain and S.C.Brown, Moving striations in a low pressure Argon discharge, Phys. Fluids **14**, 1383 (1971)

[95] V.I.Kolobov and D.J. Economou, Anomalous skin effect in gas discharge plasmas, Plasma Sources Sci. Technol. **6**, R1 (1997)

[96] V.I.Kolobov, Anomalous skin effect in bounded systems, in U.Kortshagen and L.D.Tsendin, Eds, *Electron Kinetics and Applications of Glow Discharges*, Plenum Press, New York, 1998

[97] M.M. Turner, Collisionless electron heating in an inductively coupled discharge, Phys. Rev. Lett. **71**, 1844 (1993)

[98] V.Vahedi, M.A.Lieberman, G.DiPeso, T.D.Rognlien and D.Hewett, Analytic model of power deposition in inductively coupled plasma sources, J. Appl. Phys. **78**, 1446 (1995)

[99] R.H.Cohen and T.D.Rognlien, Electron kinetics in radio-frequency magnetic fields of inductively coupled plasma sources, Plasma Sources Sci. Technol. **5**, 442 (1996)

[100] K.C.Shaing, Electron heating in inductively coupled discharges, Phys. Plasmas **3**, 3300 (1996)

[101] N.S.Yoon, S.S. Kim, C.S.Chang and D.I. Choi, One-dimensional solution for electron heating in an inductively coupled plasmas, Phys. Rev. E **54**, 757 (1996)

[102] N.S.Yoon, S.M Hwang, D.I. Choi, Two-dimensional nonlocal heating theory of planar-type inductively coupled plasma discharge, Phys. Rev. E **55**, 7536 (1997)

[103] K-I.You and N.S.Yoon, Discharge impedance of solenoidal inductively coupled plasma discharge, Phys. Rev. E **59**, 7074 (1999)

[104] S.S.Kim, C.S.Chang, N.S.Yoon, K-W.Whang, Inductively coupled plasma heating in a weakly magnetized plasma, Phys. Plasmas **6**, 2926 (1999)

[105] S-H Seo, C-W Chung, J-I Hong and H-Y Chung, Nonlocal electron kinetics in a planar inductive helium discharge, Phys. Rev. E **62**, 7155 (2000)

[106] Yu.O.Tushetsky, A.I.Smolyakov and V.A.Godyak, Plasma Sources Sci. Technol. **11**, 203 (2002)

[107] Yu.M.Aliev, I.D.Kaganovich and H.Schluter, Quasilinear theory of collisionless electron heating in rf gas discharges, Phys. Plasmas **4**, 2413 (1997)

[108] I.D.Kaganovich and O.Polomarov, Self-consistent system of equations for a kinetic description of the low-pressure discharges accounting for the nonlocal and collisionless electron dynamics, Phys. Rev. E **68**, 026411 (2003)

[109] I.D.Kaganovich, O.V.Polomarov, C.E.Theodosiou, Landau damping and and anomalous skin effect in low ressure gas discharges, Phys. Plasmas **11**, 2399 (2004)

[110] O.V.Polomarov, C.E.Theodosou, I.D.Kaganovich, Enhanced collisionless heating in a nonuniform plasma at the bounce resonance condition, Phys. Plasmas **12**, 080704 (2005)

[111] O.V.Polomarov, C.E.Theodosiou and I.D.Kaganovich, Effectiveness of electron-cyclotron and transmission resonant heating in inductively coupled plasmas, Phys. Plasmas **12** (2005)

[112] V.I.Kolobov, Lymberopoulos and Economou, Electron kinetics and non-Joule heating in near-collisionless inductively coupled plasmas, Phys. Rev. E **55**, 3408 (1997)

[113] S.Rauf and M.J.Kushner, Model of noncollisional heating in inductively coupled plasma processing sources, J. Appl. Phys. **81**, 5966 (1997)

[114] M.A. Lieberman and V.A.Godyak, From Fermi acceleration to collisionless discharge heating, IEEE Trans. Plasma Sci. **26**, 955 (1998)

[115] M.Shoucri, J.P.Matte, and A.Cote, Numerical simulation of an inductively coupled discharge using an Eulerian Vlasov code, J. Phys. D **36**, 2083 (2003)

[116] W.Liang, N.Goldsman, I.Meyergoyz, and P.Oldiges, 2-D MOSFET modeling including surface effects and impact ionization by self-consistent solution of the Boltzmann, Poisson and hole-continuity equations, IEEE Trans. Electron Dev. **44**, 257 (1997)

[117] E.Bringuier, Augmented Fokker-Planck equation for electron transport in arbitrary electric fields, J. Appl. Phys. **86**, 6847 (1999)

[118] V.Latocha, L.Garrigues, P.Degond and J.P.Boeuf, Numerical simulation of electron transport in the channel region of a stationary plasma thruster, Plasma Sources Sci. Technol.**11**, 104 (2002)

[119] M.Gutnic, M.M.Haefele, I.Paun, E.Sonnendrucker, Vlasov simulations on an adaptive phase-space grid, Comp. Phys. Comm. **164**, 214 (2004)

[120] P.Colella, M.R.Dorr, D.D.Wake, Numerical solution of plasma fluid equations using locally refined grids, J. Comp. Phys. **152**, 550 (1999)